Spring 2021

Characterization and Hydrogenation Activity of Supported Palladium Particles

Narayan Acharya

CHARACTERIZATION AND HYDROGENATION ACTIVITY OF SUPPORTED PALLADIUM PARTICLES

By

Narayan Acharya

Bachelor of Science
Tribhuvan University, 2011

Master of Science
Tribhuvan University, 2013

Submitted in Partial Fulfillment of the Requirements

For the Degree of Master of Science in

Chemistry

College of Arts and Science

University of South Carolina

2021

Accepted by:

Donna A. Chen, Major Director of Thesis

Michael L. Myrick, Reader

Tracey L. Weldon, Interim Vice Provost and Dean of the Graduate School

DEDICATION

I dedicate this work to my father, Bishnu Pd. Acharya and my late mother, Kalpana Acharya.

ACKNOWLEDGMENTS

I thank my colleagues, lab members, and collaborators at the University of South Carolina. My time and work would not have been the same without them and everyone in the projects. I greatly appreciate my major professor, Dr. Donna A. Chen, for providing opportunities for me to understand many concepts in the field of catalysis. You have given me many lessons in the lab and in classrooms that helped me grow in a small-time frame, and I express my gratitude to all my committee members for their help, guidance, knowledge, and support.

ABSTRACT

In this project, the hydrogenation activity of palladium (Pd) particles supported on different carbon and oxide supports was investigated. Supported Pd particles were prepared using strong electrostatic adsorption (SEA) technique, which is known to produce metal particles with narrow and uniform distribution. The scanning transmission electron microscopy (STEM), X-ray diffraction (XRD), and chemisorption methods were used to characterize the Pd particle size in this project. The Pd particles on different supports were annealed at a specific temperature, and the particle size was studied as a function of annealing temperature. Propylene hydrogenation to propane was conducted in a flow reactor to evaluate the catalytic performance. The smaller Pd particles were more active than the larger particles toward the hydrogenation reaction on all supports, and Pd particles on the graphene nanoplatelets were more active than on other supports. It was observed that smaller Pd particles on the carbon supports were decorated with carbon. The enhanced activity of particles supported on graphene nanoplatelets and its comparison to other catalysts as a function of particle size were studied in this project.

TABLE OF CONTENTS

LIST OF FIGURES

CHAPTER 1

INTRODUCTION

1.1 OVERVIEW

Catalysts are often required to promote the desired chemical transformations and are known to facilitate chemical reactions by lowering the activation energy. Seventy percent of all products are conducted in the presence of catalyst.[1] Catalysis is involved in several fields, such as pharmaceuticals, petroleum chemicals, commodity chemicals, and agriculture.[2] Catalytic processes are also used to facilitate more environmentally friendly processes; for example, catalytic converters are used in automobiles to decrease harmful gas emissions.[3–6] Other catalytic process applications include fuel cells, synthetic fuels, food processing, and producing fine chemicals.[8] Due to these various applications, there is a great interest in understanding catalytic activity and methods of synthesis to promote more efficient catalysts for the future.[1]

Heterogeneous catalysis plays an essential role in industrial processes. More than 90% of the commercial chemical reactions are conducted through heterogeneous catalysis.[9] Examples of industrial applications include ammonia synthesis, methanol and Fischer–Tropsch Synthesis, hydrocarbon transformation, environmental catalysis, and

hydroprocessing reactions.[10] Heterogeneous catalysts supersede homogeneous catalysts due to their reusability and ease of separation from the reaction mixture.[11] Here, the heterogeneous catalysis occurring on supported palladium (Pd) particles is considered.

1.2 SUPPORTED METAL CATALYSTS

Supported metal catalysts play a vital role in energy storage and conversion, nanoelectronics, fuel production, and chemical production.[12] Metal nanoparticles have gained attention due to their unique properties compared to their bulk counterparts. The metal nanoparticles possess a large surface-to-volume ratio and high dispersion, which makes them ideal for catalytic applications.[5]

Overall activity depends on the number of metal atoms at the surface that are accessible to reactant molecules. .[7,13–16] For metal particles that are well dispersed over high surface area supports, less metal is required for catalysis, thus decreasing the overall cost. The catalyst support also plays a vital role in providing well-dispersed metal particles. The metal catalyst support is selected based on its cost, availability, and ability to anchor the nanoparticles on the surface. Carbon is a commonly used support because of its inertness, low cost, high surface area, easy recovery of the metal phase in the spent catalyst, and low deactivation.[17,18]

1.3 PALLADIUM PARTICLE AS CATALYST

Pd catalysts are used in petroleum cracking, oxidation of organics, C–C bond formation reactions, coupling reactions, and alcohol oxidation.[19] Palladium based catalysts are considered one of the most promising catalysts for the hydrogenation of alkenes and alkynes. For example, palladium supported on silica catalysts has shown remarkably high activity in the hydrogenation of benzene, 1-hexene, cyclohexene, and benzonitrile.[20] Being less costly than other metals like Pt and Rh, it is one of the most studied metal particles to improve catalytic activity. Most importantly, the property of Pd to catalyze different reactions makes it a widely used industrial catalytic converter. Pd mixed with Rh and Pt forms a three-way catalyst (TWC), which can neutralize unburned hydrocarbons, nitrogen oxides, and CO. However, the higher cost of Rh and Pt, and the scarce availability of Rh, directed the research toward using only Pd three-way catalysts.[21] Studies in the literature have shown that catalytic activity of the supported Pd particles depends on the particle size, dispersion, and the method in which the nanoparticles are deposited with stability against agglomeration. [22,23] Very recently, Pd deposited on single-wall carbon nanotubes has demonstrated excellent activity toward the Heck and Suzuki coupling reactions.[23] The graphene supported Pd catalysts prepared using strong electrostatic adsorption and microwaved irradiation (SEA-MW) are highly active toward the coupling reaction.[17] The catalytic activity of graphene supported Pd catalyst, commercially available Pd on activated carbon and Pd on activated charcoal, is properly compared by the coupling reaction between 4-bromotoluene and phenyl boronic acid to produce 4-methyl 1, 1'- biphenyl. The result

reported showed that the turn over frequency (TOF) of the Pd on graphene catalyst is at least one order magnitude higher than its other counterparts.[17]

In this work, supported Pd particles were subjected to the propylene hydrogenation reaction for catalytic testing. Catalytic hydrogenation of unsaturated organic molecules is used extensively in the chemical industry for various applications, such as in the petroleum refining industry, production of pharmaceuticals, agrochemicals, and flavors and fragrances.[24]

1.4 CATALYST PREPARATION

Improved catalytic synthesis methods are desired to prepare catalysts with high dispersion, control over particle morphology, and good stability. The control in the size and dispersion enhance the catalytic activities.[5] There are several techniques for catalyst preparation, such as ion exchange (IE), wet impregnation (WI), dry impregnation (DI), deposition precipitation, reactive adsorption, chemical vapor deposition, and incipient wetness impregnation(IWI).[9] However, in these techniques, there is a non-uniform distribution of the metal on the support surface. This leads to poor control over metallic dispersion and surface atoms.[9]

1.5 IMPREGNATION TECHNIQUE

The impregnation technique is a common and low-cost technique to produce metal nanoparticles on support.[14] In this method, a specific volume of a metal precursor solution is placed in contact with the support material for a specific period. The concentration of metal on the support depends on the mixing and drying process. A

reduction treatment is required to obtain stable metal particles from the precursor metal ions. By reduction, hydrogen induces the formation of metallic species. The impregnation methods are divided into IWI and WI depending on the volume of the solution.[14]

1.6 STRONG ELECTROSTATIC ADSORPTION (SEA)

SEA is a specific type of WI in which the final pH is targeted to the range in which adsorption is most substantial. Using the SEA method, supported metal nanoparticles are synthesized with small sizes and uniform size distributions.[25–30] This method's hypothesis is that adsorption of a monolayer of the metal complexes via electrostatic adsorption induces the distribution of small uniform particles.[31] This idea was presented to the catalysis community in 1978 by Brunelle[32] and further developed by Schwarz.[33] They postulated that there is electrostatic interaction induced between the oppositely charged metal precursor ions and support. This condition is achieved by controlling the final pH of the impregnating solution about the point of zero charge (PZC) of the support materials.

Finding the PZC is crucial for determining the SEA conditions.[14,25,34,35] The PZC is found at the isoelectric point, where there is no charge on the support surface. For oxide support, the PZC is the pH at which the hydroxyl groups overall are neutral.[7,14,34] As pH is adjusted away from the PZC, the surface's functional groups are protonated or deprotonated depending on if the pH is below or above the PZC, respectively. The cationic or anionic precursor is deposited based on the protonation or deprotonation of

the support surface. The strong interaction between the support and precursor prevents nanoparticle agglomeration and migration during the drying process.[29,35–37]

Oxides adsorb the anionic complexes at pH below the PZC of the support, where the surface is protonated and positively charged.[14,38] To promote adsorption, the pH of the precursor solution was carefully adjusted. Then, metal ions are adsorbed on the surface by the electrostatic force of attraction. Different steps involved in the SEA method are given in the figure below, and Figure 1.1 shows the SEA mechanism.[39]

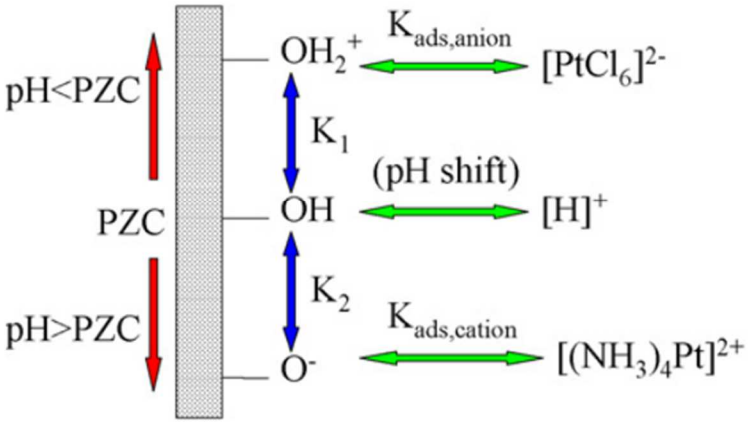

Figure 1.1: Mechanism of SEA technique illustrating surface charging, protonation, deprotonation, and adsorption.[37]

After determining the PZC of the support, a precursor was chosen, and an uptake survey was conducted. The uptake survey was performed to determine the optimal pH. Then, this pH related to maximum adsorption was defined as an optimal pH, where the highest adsorption of the metal precursor on the support was obtained. This optimal pH is called the point of maximum adsorption. Once the uptake survey was completed, the optimal pH was used to adsorb the precursor into the support.

Figure 1.2 below is an adsorption survey of Pd nanoparticles on silica via SEA.[39] The highest adsorption of Pd particles occurred at pH ~11.5. Initially, from pH 1–5, no adsorption was observed. As the solution's pH increased, the support surface deprotonated, and the cationic Pd complex started to adsorb electrostatically at pH 6. At extreme pH values, no adsorption was observed due to high ionic strength.[40] The higher ionic strength was due to the excess ions, which caused double layer compression or electrical screening, thereby decreasing the adsorption equilibrium constant for metal complexes.[40]

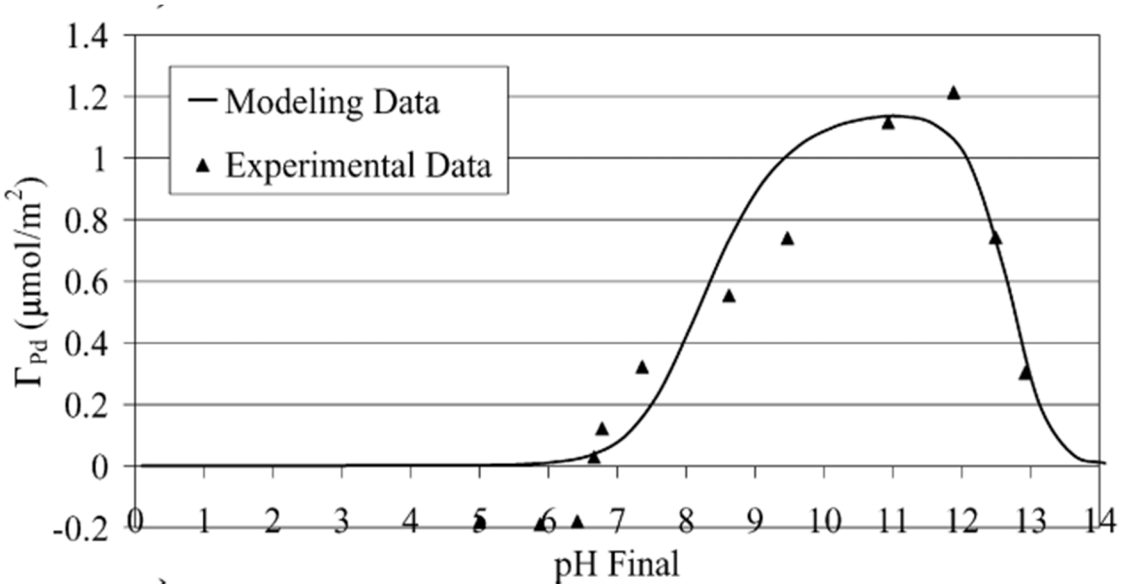

Figure 1.2: Metal surface density as a function of pH final for tetraamine Pd(II) complex on silica support.[39]

CHAPTER 2

SYNTHESIS, CHARACTERIZATION, AND HYDROGENATION ACTIVITY OF PD ON CARBON AND OXIDES SUPPORTS

2.1 INTRODUCTION

The properties of supported metal nanoparticles are influenced by their shape, size, oxidation state, and metal support interactions. [41] In structure-sensitive reactions, nanoparticle size is an important factor in catalytic activity. Schlatter and Boudart[42] reported that the rate of ethene hydrogenation is independent of Pt particle size. However, Shaikhutdinov *et al.* [43] reported that ethylene hydrogenation activity is independent of particle size between 1–6 nm. In contrast to these studies, Borodziniski[44] reported that for ethylene hydrogenation over the Pd/SiO_2 catalysts, the particle diameter over a range of 4.2–26.2 nm does not influence the reaction mechanism and adsorption strength of the ethylene. In another study, Gigola[45] observed an increase in TOF with an increase in the particle size for Pd/ SiO_2 catalyst for ethylene hydrogenation in the range of 3–8 nm. Binder[46] concluded that discrepancies in the literature could be due to differences in reaction conditions.

The catalyst support can also play an important role through controlling the size, morphology, and electronic properties of the particles.[47] For example, Pd nanoparticles supported on graphitic nanoplatelets show exceptionally high activity in the Suzuki coupling reaction.[17] This work is focused on the preparation of Pd particles with controlled sizes on silica and carbon supports and the study of the catalytic activity of these materials in propylene hydrogenation reactions.

2.2 EXPERIMENTAL

2.2.1 Synthesis

Catalyst preparation:

Catalysts were prepared by the SEA method using a cationic metal precursor, palladium (II) tetraamine nitrate (PdTA-NO_3), at basic pH. The metal precursor was purchased from Sigma Aldrich with a purity of 99.999% and used without any additional treatment. Vulcan XC72 (VXC72) was purchased from Cabot Corporation, graphene nanoplatelets from Alfa Aesar, referred to as GN-Alfa, and OX50 silica is from Aerosil. The carbon supports were oxidized in concentrated nitric acid (> 67%) at 90°C for 3 h and washed until their pH reached that of DI water. Oxidized VXC72 (oxdVXC2) and oxidized GN-Alfa (oxdGN-Alfa) were pre-annealed at 600°C for 4 h in helium gas using a heating ramp rate of 10°C/min and a gas flow of 600 SCCM. The OX50 support was pre-annealed at 800°C for 4 h under the same conditions. These catalyst supports were designated as OX50(800), oxdVXC72(600), and oxdGN-Alfa(600) to specify the pre-annealing temperature.

The PZC and surface area of all supports were determined before metal deposition. The PZC of silica was 4.1, GN-Alfa was 4.2, oxdVXC72 was 2.5, oxdGN-Alfa was 1.3, and oxdGN-Alfa(600) was 6.5. The BET surface area of OX50 was 50 m^2/gm, oxdVXC-72 was 230 m^2/gm, and oxdGN-Alfa was 230 m^2/gm.

The uptake surveys were conducted on these carbon and oxide supports to determine the pH at which the support's metal adsorption is maximum. The uptake of the metal precursor was found to be maximum at pH value higher than the PZC. Then, this pH related to maximum adsorption was defined as an optimal pH. The optimal pH determined was used for the precursor adsorption on the supports. The survey was performed on several pH values higher than the PZC in the basic pH range. For the survey, ~20 ml of precursor solutions was prepared for each pH value in the range of 1–13, and the mass of the support was chosen based on the support surface area and desired surface loading. The detailed relationship between support surface area, surface loading, the volume of solution, and the mass of the support was used is found elsewhere.[14,35] The pH of the solutions was adjusted by adding HCl, NH_4OH, and NaOH. A surface loading of 1000 m^2/L was used as a set standard SEA parameter for all supports. All supports were added to the precursor solutions and mechanically shaken at 120 rpm speed for an hour. The metal uptake at different pH levels was then determined by calculating the initial and final concentrations by ICP-OES. The pH for maximum adsorption was determined, which was used as the optimized pH value for the catalyst synthesis. The optimal pH for the GN-Alfa was found to be 11.8, silica was 12, oxdGN-Alfa (600) was 11.15, and other support like oxdVXC72(600) was 10, as

reported elsewhere.[48] Following catalyst synthesis, the catalysts were dried in an oven at 120°C for 16 h and then reduced at 180°C for 1 h in 10% H_2/He. ICP-OES was conducted to calculate the Pd weight % from the initial and the final concentrations of the metal precursor solutions. The weight loading of the catalyst was 0.39% for Pd/OX50(800), 0.5% for Pd/oxdVXC72(600), and 0.1% for Pd/oxdGN-Alfa(600).

After the Pd precursors were reduced to metallic particles, the catalysts were annealed at different temperatures to prepare particles of different sizes. The Pd/OX50(800) catalyst was annealed at 600°C, 700°C, and 800°C, and the Pd/carbon(600) catalysts were annealed at 400°C, 500°C, and 600°C. All catalysts were heated in a flow of 600 SCCM of He for 4 h.

2.2.2 Characterization

Pulse chemisorption:

The number of Pd sites for the catalysts and particle sizes were determined by hydrogen titration of oxygen pre-covered surfaces using a Micromeritics Autochem II 2920 automated analyzer. The catalyst was initially reduced *in situ* in flowing 10% H_2/Ar at 200°C for 2 h. After reduction, the catalyst was oxidized in 10% O_2/He for 30 min at 40°C, and 10% H_2/Ar pulses were introduced to remove the oxygen from the surface in the form of water at 40°C. The amount of hydrogen consumed in this process was measured using a thermal conductivity detector (TCD). An average value was calculated from the three successive titrations. The stoichiometry of the chemisorption was 0.667

surface Pd atom: 1 H_2 molecule. The particle diameters were calculated assuming a hemispherical geometry.

X-ray diffraction (XRD):

X-ray diffraction measurements on supported Pd-catalysts were performed on Rigaku Miniflex II, a benchtop system equipped with a D/teX-Ultra silicon strip detector and a Cu Kα radiation (λ = 1.5406 Å) operated at 30 mA and 15 kV. All XRD data were collected at 0.05°/min and a sampling width of 0.02°.[49] The background signal from the support was subtracted from the diffraction pattern. Diffraction peaks were fit using Fityk software with Gaussian line shapes. The particle sizes were calculated from the Scherrer equation using full width at half maximum (FWHM) values from the fits.[50]

$$\mathrm{P} = \frac{K\,\lambda}{b\,cos\theta} \qquad (2.1)$$

The particle size is calculated using equation 2.1, where P is the actual particle size, *K* is a constant related to the crystallite shape with a value of 0.9, λ is the wavelength of Cu Kα radiation, *b* is the peak width after subtracting the instrumental peak width, and the θ is the Bragg angle.

Scanning transmission electron microscopy (STEM)

The particle sizes were measured using JEOL 2100F 200 kV STEM. Catalysts were suspended in isopropanol and dispersed on a holey carbon-coated copper grid. Approximately 100–500 particles were counted for each catalyst. The following average values were determined: the average number diameter(d_n) = $\sum n_i d_i / \sum n_i$, surface average

diameter(d_s) = $\sum n_i d_i^3 / \sum n_i d_i^2$, and the volume average diameter(d_v) = $\sum n_i d_i^4 / \sum n_i d_i^3$, where n_i is the number of particles with diameter d_i.[51]

Catalyst evaluation:

The supported metal catalysts in this project were tested for propylene hydrogenation. Catalyst evaluation was performed in a fixed bed flow reactor equipped with a Hewlett-Packard 5890 Series II chromatograph with an HP-PLOT Q capillary column and a flame ionization detector. This system has been described extensively elsewhere.[52] Approximately 0.001–0.005 grams of catalyst was mixed with 0.025 grams of Al_2O_3 and supported by glass wool in the stainless reactor tube. The samples were reduced at 200°C for 2 h in 10% H_2/He and then cooled to the reaction temperature of −5°C. The feed gas compositions were 5 SCCM propylene, 20SCCM H_2, and 75 SCCM He.

2.4 RESULTS AND DISCUSSION

2.4.1 Palladium particle size as a function of annealing temperature

Figure 2.1 shows the Pd particle size for the Pd/OX50(800) catalyst as a function of annealing temperature (600°C, 700°C, and 800°C), as determined by these three different experimental methods. For the OX50 support, the unannealed Pd particles were below 2 nm in all cases. After annealing at 600°C, the STEM and chemisorption particle sizes were the same. No Pd peak could be detected in PXRD, and an upper limit on particle size was set to 1.5 nm, which was the smallest Pd diameter detected by XRD. After annealing at 700°C, the average STEM size was 3.7 nm, and the chemisorption size

had a similar value of 4.4 nm. When the catalyst was annealed at 800°C, the discrepancy between the chemisorption and STEM was still below 30%. Therefore, Pd particle sizes measured by chemisorption, XRD, and STEM for the Pd on the OX50(800) catalyst are agreed.

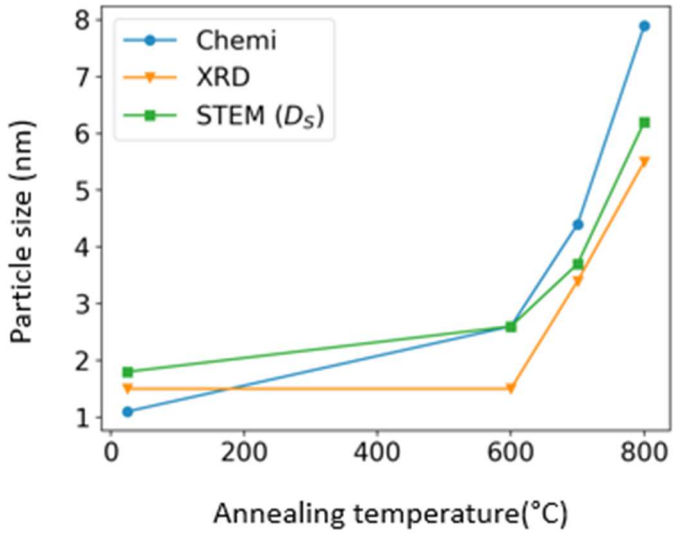

Figure 2.1: Particle size as a function of annealing temperature for Pd on OX50(800) catalysts.

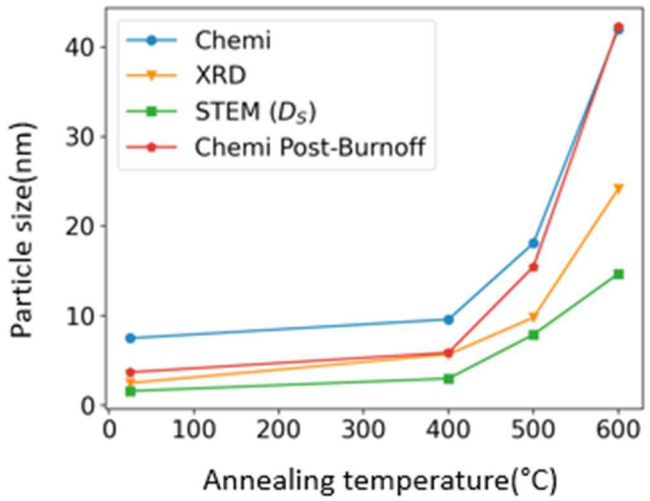

Figure 2.2: Particle size as a function of annealing temperature for Pd on oxdVXC72(600) catalysts.

Figure 2.2 shows the particle size characterization by chemisorption, XRD, and STEM experiments for Pd on oxdVXC72(600) catalysts after annealing at 400°C, 500°C, and 600°C. Unlike for silica-supported Pd particles, a significant difference in size measured by chemisorption and STEM was observed. For the unannealed catalyst, the difference was 300% between these two techniques. However, STEM and XRD are agreed. The larger chemisorption particle size is believed to be due to the carbon decoration on the Pd particles. After removing the carbon, by heating in oxygen (carbon burnoff treatment), the difference was reduced to ~50% for the unannealed catalyst, ~10% for the 400°C annealed catalyst, < 60% for the 500°C annealed catalyst, and no change was observed for the 600°C annealed catalyst. This indicated that Pd on the oxdVXC72 support was highly decorated by carbon for the unannealed and 400°C annealed catalysts.

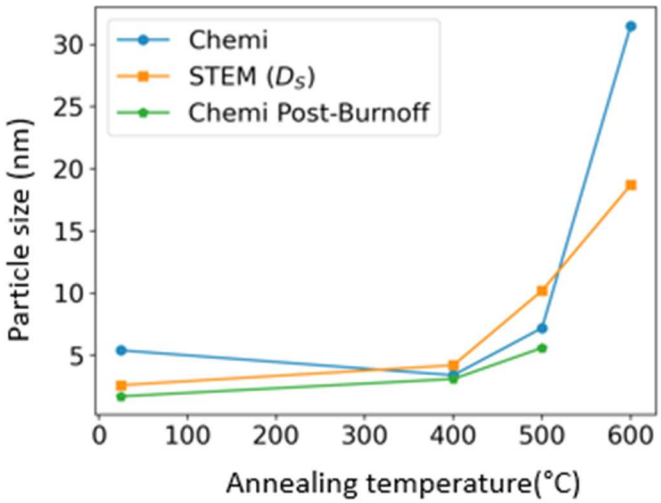

Figure 2.3: Particle size as a function of annealing temperature for Pd on oxdGN-Alfa(600) catalysts.

Figure 2.3 shows the Pd particle sizes measured by STEM and chemisorption experiments for Pd on oxdGN-Alfa catalysts annealed at different temperatures. Note that the Pd peak could not be detected by XRD due to the low weight loading. The unannealed Pd particles on the oxdGN-Alfa support were ~5 nm, as measured by chemisorption. This particle size significantly exceeded that of the ~2 nm determined by STEM measurements. After the carbon burnoff treatment, the chemisorption particle size decreased to 1.7 nm. After annealing at 400°C, the chemisorption particle size was 3.4 nm and did not appear to be decorated by carbon, given that the pre-burnoff, post-burnoff, and STEM particle sizes were similar. After annealing to 500°C, the STEM particle size exceeded the chemisorption size, but the difference was not large compared to the unannealed particles. After annealing at 600°C, the chemisorption particle size was 31.5 nm, and the STEM size was 18.5 nm. This difference in STEM could be attributed to the broad Pd particle size distribution for the 600°C annealed catalyst. The difference between small Pd particles by chemisorption and STEM particle size was due to the carbon decoration in the annealed Pd particles.

3.4.2 Propylene hydrogenation

Figures 2.4, 2.5, and 2.6 show the TOF for product formation vs. time on stream for propylene hydrogenation on Pd particles on the three different supports. TOF was calculated from the measured rate of reaction and the number of active sites determined from the chemisorption experiments.

For the Pd/OX50(800), the unannealed catalyst had the highest initial TOF at ~35 s^{-1}, which gradually decreased to 21 s^{-1} at the end of 24 h of reaction. For the catalysts annealed at 600°C and 700°C, the TOF values decreased to~12–15 s^{-1} after 24 h of on stream. The TOF for the 800°C annealed catalyst was ~10 s^{-1} after 24 h on stream.

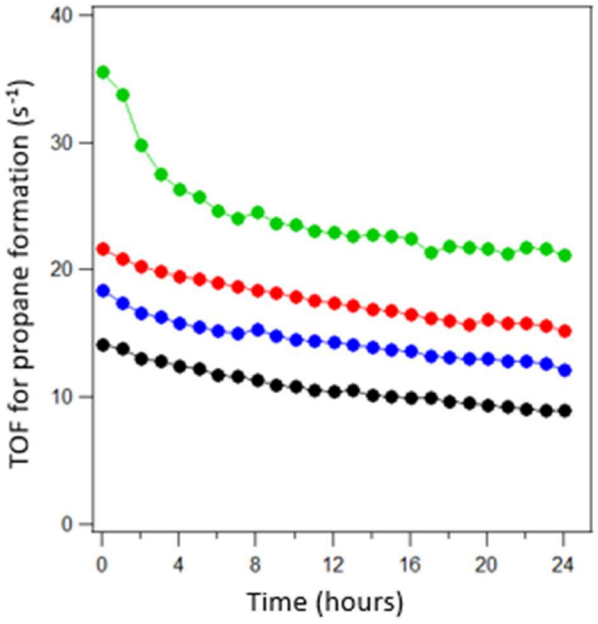

Figure 2.4: Propane formation as a function of time on stream for Pd/OX50(800) catalysts: unannealed (green), annealed at 600°C (blue), annealed at 700°C (red), and annealed at 800°C (black).

Figure 2.5 shows the TOF as a function of time on stream for the Pd particles on the oxdVXC72(600) support. The TOF for the unannealed catalyst was the highest. Initially, the TOF was ~29 s^{-1} and then gradually decreased to ~20 s^{-1} at 24 hours. The TOFs for the 400°C and 500°C catalysts were almost identical after 24 h of reaction (~16 s^{-1}). The 600°C annealed catalyst had the lowest TOF, which was ~10 s^{-1} after 24 h.

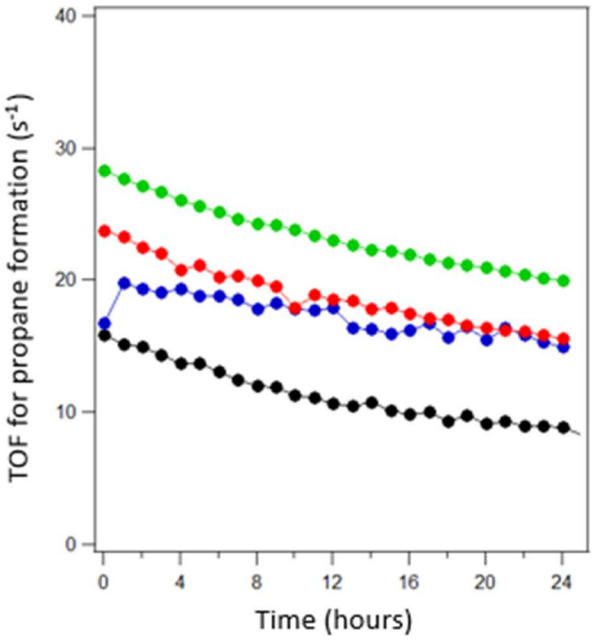

Figure 2.5: Propane formation as a function of time on stream for Pd/oxdVXC72(600) catalysts: unannealed (green), annealed at 400°C (red), annealed at 500°C (blue), annealed at 600°C (black).

Figure 2.6 shows the TOF vs. time on stream for Pd particles supported on oxdGN-Alfa(600). For the Pd/oxdGN-Alfa(600) catalyst, the unannealed catalyst had the highest activity, and annealing at a higher temperature decreased the activity. However, the activity of the annealed catalyst was constant over time compared to the unannealed catalyst. For the 600°C annealed catalyst, the activity was significantly lower. The unannealed catalyst had about 5-fold higher initial activity than the 400°C annealed catalyst. For the 500°C annealed catalyst, the TOF was like that of the 400°C annealed catalyst.

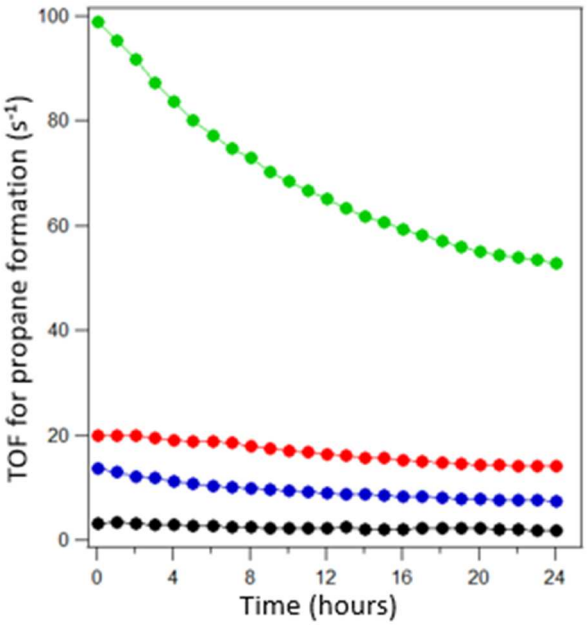

Figure 2.6: Propane formation as a function of time on stream for Pd/oxdGN-Alfa(600) catalysts: unannealed (green), annealed at 400°C (red), annealed at 500°C (blue), annealed at 600°C (black).

2.5 CONCLUSION

A clear particle size effect was demonstrated for the propylene hydrogenation reaction on Pd/OX50. The smaller Pd nanoparticles exhibited higher activity compared to larger Pd particles. However, particle size effects were more difficult to understand on the carbon-supported catalysts due to carbon decoration. This carbon decoration was observed for all sizes of Pd particles on oxdVXC72 and the smaller particles on oxdGN-Alfa. The Pd nanoparticles on the GN-Alfa support exhibited excellent activities compared to similar sized-Pd particles on other silica and carbon supports. This result suggests that the GN-Alfa support enhances the hydrogenation activity of Pd particles.

2.6 ACKNOWLEDGMENTS

I would like to thank the Center for Rational Catalyst Synthesis, which is funded by a National Science Foundation Industry/University Collaborative Research Center Grant (IIP 1464595), for financial support. I would also like to thank my lab mate Deependra Shakya for his help with the propylene hydrogenation experiments and Dr. Ritubarna Banerjee for conducting the XRD and STEM studies. Also, I would like to thank Dr. JR Regalbuto for allowing me to work in his lab and his group members for help and support during the work.

REFERENCES

(1) Deutschmann, O.; Knözinger, H.; Kochloefl, K.; Turek, T. Heterogeneous Catalysis and Solid Catalysts, 3. Industrial Applications. In *Ullmann's Encyclopedia of Industrial Chemistry*; Wiley-VCH Verlag GmbH & Co. KGaA, Ed.; Wiley-VCH Verlag GmbH & Co. KGaA: Weinheim, Germany, 2011; p o05_o03. https://doi.org/10.1002/14356007.o05_o03.

(2) Economic Importance of Catalysts. In *Industrial Catalysis*; Wiley-VCH Verlag GmbH & Co. KGaA: Weinheim, Germany, 2015; pp 459–462. https://doi.org/10.1002/9783527684625.ch17.

(3) Economic Importance of Catalysts. In *Industrial Catalysis*; Wiley-VCH Verlag GmbH & Co. KGaA: Weinheim, Germany, 2015; pp 459–462. https://doi.org/10.1002/9783527684625.ch17.

(4) He, L.; Weniger, F.; Neumann, H.; Beller, M. Synthesis, Characterization, and Application of Metal Nanoparticles Supported on Nitrogen-Doped Carbon: Catalysis beyond Electrochemistry. *Angew. Chem. Int. Ed.* **2016**, *55* (41), 12582–12594. https://doi.org/10.1002/anie.201603198.

(5) Campelo, J. M.; Luna, D.; Luque, R.; Marinas, J. M.; Romero, A. A. Sustainable Preparation of Supported Metal Nanoparticles and Their Applications in Catalysis. *ChemSusChem* **2009**, *2* (1), 18–45. https://doi.org/10.1002/cssc.200800227.

(6) White, R. J.; Luque, R.; Budarin, V. L.; Clark, J. H.; Macquarrie, D. J. Supported Metal Nanoparticles on Porous Materials. Methods and Applications. *Chem Soc Rev* **2009**, *38* (2), 481–494. https://doi.org/10.1039/B802654H.

(7) Brunelle, J. P. Preparation of Catalysts by Metallic Complex Adsorption on Mineral Oxides. *Pure Appl. Chem.* **1978**, *50* (9–10), 1211–1229. https://doi.org/10.1351/pac197850091211.

(8) Campelo, J. M.; Luna, D.; Luque, R.; Marinas, J. M.; Romero, A. A. Sustainable Preparation of Supported Metal Nanoparticles and Their Applications in Catalysis. *ChemSusChem* **2009**, *2* (1), 18–45. https://doi.org/10.1002/cssc.200800227.

(9) Wegener, S. L.; Marks, T. J.; Stair, P. C. Design Strategies for the Molecular Level Synthesis of Supported Catalysts. *Acc. Chem. Res.* **2012**, *45* (2), 206–214. https://doi.org/10.1021/ar2001342.

(10) Deutschmann, O.; Knözinger, H.; Kochloefl, K.; Turek, T. Heterogeneous Catalysis and Solid Catalysts, 3. Industrial Applications. In *Ullmann's Encyclopedia of Industrial Chemistry*; Wiley-VCH Verlag GmbH & Co. KGaA, Ed.; Wiley-VCH Verlag GmbH & Co. KGaA: Weinheim, Germany, 2011; p o05_o03. https://doi.org/10.1002/14356007.o05_o03.

(11) Thomas, S. J. M. The Advantages of Exploring the Interface Between Heterogeneous and Homogeneous Catalysis. *ChemCatChem* **2010**, *2* (2), 127–132. https://doi.org/10.1002/cctc.200900275.

(12) Prieto, G.; Zečević, J.; Friedrich, H.; de Jong, K. P.; de Jongh, P. E. Towards Stable Catalysts by Controlling Collective Properties of Supported Metal Nanoparticles. *Nat. Mater.* **2013**, *12* (1), 34–39. https://doi.org/10.1038/nmat3471.

(13) *Catalyst Preparation: Science and Engineering*; Regalbuto, J. R., Ed.; Taylor & Francis: Boca Raton, 2007.
(14) *Catalyst Preparation: Science and Engineering*; Regalbuto, J. R., Ed.; Taylor & Francis: Boca Raton, 2007.
(15) Banerjee, R.; Liu, Q.; Tengco, J. M. M.; Regalbuto, J. R. Detection of Ambient Oxidation of Ultrasmall Supported Platinum Nanoparticles with Benchtop Powder X-Ray Diffraction. *Catal. Lett.* **2017**, *147* (7), 1754–1764. https://doi.org/10.1007/s10562-017-2060-2.
(16) Ritubarna Banerjee; Jose Contreras-Mora; Susan McQuiston; Brandon Bolton; Bahareh Tavakoli Mehrabadi; John Regalbuto. Electrostatic Adsorption of Platinum onto Carbon Nanotubes and Nanofibers for Nanoparticle Synthesis. *C* **2018**, *4* (1), 12. https://doi.org/10.3390/c4010012.
(17) Gilliland, S. E.; Tengco, J. M. M.; Yang, Y.; Regalbuto, J. R.; Castano, C. E.; Gupton, B. F. Electrostatic Adsorption-Microwave Synthesis of Palladium Nanoparticles on Graphene for Improved Cross-Coupling Activity. *Appl. Catal. Gen.* **2018**, *550*, 168–175. https://doi.org/10.1016/j.apcata.2017.11.007.
(18) Auer, E.; Freund, A.; Pietsch, J.; Tacke, T. Carbons as Supports for Industrial Precious Metal Catalysts. *Appl. Catal. Gen.* **1998**, *173* (2), 259–271. https://doi.org/10.1016/S0926-860X(98)00184-7.
(19) Saldan, I.; Semenyuk, Y.; Marchuk, I.; Reshetnyak, O. Chemical Synthesis and Application of Palladium Nanoparticles. *J. Mater. Sci.* **2015**, *50* (6), 2337–2354. https://doi.org/10.1007/s10853-014-8802-2.
(20) Domínguez-Quintero, O. Silica-Supported Palladium Nanoparticles Show Remarkable Hydrogenation Catalytic Activity. *J. Mol. Catal. Chem.* **2003**, *197* (1–2), 185–191. https://doi.org/10.1016/S1381-1169(02)00583-6.
(21) Decarolis, D. Effect of Precious Metal Particle Size and Support Type on Catalytic Activity as Revealed by X-ray Methods. 225.
(22) Wilson, O. M.; Knecht, M. R.; Garcia-Martinez, J. C.; Crooks, R. M. Effect of Pd Nanoparticle Size on the Catalytic Hydrogenation of Allyl Alcohol. *J. Am. Chem. Soc.* **2006**, *128* (14), 4510–4511. https://doi.org/10.1021/ja058217m.
(23) Corma, A.; Garcia, H.; Leyva, A. Catalytic Activity of Palladium Supported on Single Wall Carbon Nanotubes Compared to Palladium Supported on Activated Carbon. *J. Mol. Catal. Chem.* **2005**, *230* (1–2), 97–105. https://doi.org/10.1016/j.molcata.2004.11.030.
(24) Genet, J.-P. Asymmetric Catalytic Hydrogenation. Design of New Ru Catalysts and Chiral Ligands: From Laboratory to Industrial Applications. *Acc. Chem. Res.* **2003**, *36* (12), 908–918. https://doi.org/10.1021/ar020152u.
(25) Jiao, L.; Regalbuto, J. R. The Synthesis of Highly Dispersed Noble and Base Metals on Silica via Strong Electrostatic Adsorption: I. Amorphous Silica. *J. Catal.* **2008**, *260* (2), 329–341. https://doi.org/10.1016/j.jcat.2008.09.022.
(26) Liu, Q.; Joshi, U. A.; Über, K.; Regalbuto, J. R. The Control of Pt and Ru Nanoparticle Size on High Surface Area Supports. *Phys Chem Chem Phys* **2014**, *16* (48), 26431–26435. https://doi.org/10.1039/C4CP02714K.
(27) Zhang, L.; Liu, H.; Huang, X.; Sun, X.; Jiang, Z.; Schlögl, R.; Su, D. Stabilization of Palladium Nanoparticles on Nanodiamond-Graphene Core-Shell Supports for CO Oxidation. *Angew. Chem. Int. Ed.* **2015**, *54* (52), 15823–15826. https://doi.org/10.1002/anie.201507821.
(28) Job, N.; Lambert, S.; Zubiaur, A.; Cao, C.; Pirard, J.-P. Design of Pt/Carbon Xerogel Catalysts for PEM Fuel Cells. *Catalysts* **2015**, *5* (1), 40–57. https://doi.org/10.3390/catal5010040.

(29) Banerjee, R.; Chen, D. A.; Karakalos, S.; Piedboeuf, M.-L. C.; Job, N.; Regalbuto, J. R. Ambient Oxidation of Ultrasmall Platinum Nanoparticles on Microporous Carbon Catalyst Supports. *ACS Appl. Nano Mater.* **2018**, *1* (10), 5876–5884. https://doi.org/10.1021/acsanm.8b01548.
(30) Hao, X.; Spieker, W. A.; Regalbuto, J. R. A Further Simplification of the Revised Physical Adsorption (RPA) Model. *J. Colloid Interface Sci.* **2003**, *267* (2), 259–264. https://doi.org/10.1016/S0021-9797(03)00644-1.
(31) Jiao, L.; Regalbuto, J. R. The Synthesis of Highly Dispersed Noble and Base Metals on Silica via Strong Electrostatic Adsorption: I. Amorphous Silica. *J. Catal.* **2008**, *260* (2), 329–341. https://doi.org/10.1016/j.jcat.2008.09.022.
(32) Brunelle, J. P. Preparation of Catalysts by Metallic Complex Adsorption on Mineral Oxides. *Pure Appl. Chem.* **1978**, *50* (9–10), 1211–1229. https://doi.org/10.1351/pac197850091211.
(33) Schwarz, J. A.; Contescu, Cristian.; Contescu, Adriana. Methods for Preparation of Catalytic Materials. *Chem. Rev.* **1995**, *95* (3), 477–510. https://doi.org/10.1021/cr00035a002.
(34) Mehrabadi, B. A. T.; Eskandari, S.; Khan, U.; White, R. D.; Regalbuto, J. R. A Review of Preparation Methods for Supported Metal Catalysts. In *Advances in Catalysis*; Elsevier, 2017; Vol. 61, pp 1–35. https://doi.org/10.1016/bs.acat.2017.10.001.
(35) Cho, H.-R.; Regalbuto, J. R. The Rational Synthesis of Pt-Pd Bimetallic Catalysts by Electrostatic Adsorption. *Catal. Today* **2015**, *246*, 143–153. https://doi.org/10.1016/j.cattod.2014.09.029.
(36) *Catalyst Preparation: Science and Engineering*; Regalbuto, J. R., Ed.; Taylor & Francis: Boca Raton, 2007.
(37) Jiao, L.; Regalbuto, J. R. The Synthesis of Highly Dispersed Noble and Base Metals on Silica via Strong Electrostatic Adsorption: II. Mesoporous Silica SBA-15. *J. Catal.* **2008**, *260* (2), 342–350. https://doi.org/10.1016/j.jcat.2008.09.023.
(38) Jiao, L.; Zha, Y.; Hao, X.; Regalbuto, J. R. Simple, Scientific Syntheses with Common Catalyst Precursors. In *Studies in Surface Science and Catalysis*; Elsevier, 2006; Vol. 162, pp 211–218. https://doi.org/10.1016/S0167-2991(06)80909-2.
(39) Jiao, L.; Regalbuto, J. R. The Synthesis of Highly Dispersed Noble and Base Metals on Silica via Strong Electrostatic Adsorption: I. Amorphous Silica. *J. Catal.* **2008**, 13.
(40) Shah, A. M.; Regalbuto, J. R. Retardation of Platinum Adsorption over Oxide Supports at PH Extremes: Oxide Dissolution or High Ionic Strength? *Langmuir* **1994**, *10* (2), 500–504. https://doi.org/10.1021/la00014a026.
(41) Lokteva, E. S.; Golubina, E. V. Metal-Support Interactions in the Design of Heterogeneous Catalysts for Redox Processes. *Pure Appl. Chem.* **2019**, *91* (4), 609–631. https://doi.org/10.1515/pac-2018-0715.
(42) Schlatter1972.Pdf.
(43) Shaikhutdinov, S.; Heemeier, M.; Bäumer, M.; Lear, T.; Lennon, D.; Oldman, R. J.; Jackson, S. D.; Freund, H.-J. Structure–Reactivity Relationships on Supported Metal Model Catalysts: Adsorption and Reaction of Ethene and Hydrogen on Pd/Al2O3/NiAl(110). *J. Catal.* **2001**, *200* (2), 330–339. https://doi.org/10.1006/jcat.2001.3212.
(44) Borodziński2001_Article_TheEffectOfPalladiumParticleSi.Pdf.
(45) Gigola, C. E.; Aduriz, H. R.; Bodnariuk, P. Particle Size Effect in the Hydrogenation of Acetylene under Industrial Conditions. *Appl. Catal.* **1986**, *27* (1), 133–144. https://doi.org/10.1016/S0166-9834(00)81052-0.

(46) Binder, A.; Seipenbusch, M.; Muhler, M.; Kasper, G. Kinetics and Particle Size Effects in Ethene Hydrogenation over Supported Palladium Catalysts at Atmospheric Pressure. *J. Catal.* **2009**, *268* (1), 150–155. https://doi.org/10.1016/j.jcat.2009.09.013.
(47) Liu, L.; Corma, A. Metal Catalysts for Heterogeneous Catalysis: From Single Atoms to Nanoclusters and Nanoparticles. *Chem. Rev.* **2018**, *118* (10), 4981–5079. https://doi.org/10.1021/acs.chemrev.7b00776.
(48) Banerjee, R. The Oxidation and Decoration Chemistry of Platinum and Palladium nanoparticles on Carbon Supports. 122.
(49) Cho, H.-R.; Regalbuto, J. R. The Rational Synthesis of Pt-Pd Bimetallic Catalysts by Electrostatic Adsorption. *Catal. Today* **2015**, *246*, 143–153. https://doi.org/10.1016/j.cattod.2014.09.029.
(50) Holzwarth, U.; Gibson, N. The Scherrer Equation versus the "Debye-Scherrer Equation." *Nat. Nanotechnol.* **2011**, *6* (9), 534–534. https://doi.org/10.1038/nnano.2011.145.
(51) Datye, A. K.; Xu, Q.; Kharas, K. C.; McCarty, J. M. Particle Size Distributions in Heterogeneous Catalysts: What Do They Tell Us about the Sintering Mechanism? *Catal. Today* **2006**, *111* (1–2), 59–67. https://doi.org/10.1016/j.cattod.2005.10.013.
(52) Shakya, D. M.; Ejegbavwo, O. A.; Rajeshkumar, T.; Senanayake, S. D.; Brandt, A. J.; Farzandh, S.; Acharya, N.; Ebrahim, A. M.; Frenkel, A. I.; Rui, N.; Tate, G. L.; Monnier, J. R.; Vogiatzis, K. D.; Shustova, N. B.; Chen, D. A. Selective Catalytic Chemistry at Rhodium(II) Nodes in Bimetallic Metal–Organic Frameworks. *Angew. Chem. Int. Ed.* **2019**, *58* (46), 16533–16537. https://doi.org/10.1002/anie.201908761.